

Crystalline misfit-angle implications for solid sliding

Nicola Manini^{a,*}, O.M. Braun^{b,**}

^a*Dipartimento di Fisica, Università degli Studi di Milano,
Via Celoria 16, 20133 Milano, Italy*

^b*Institute of Physics, National Academy of Sciences of Ukraine,
46 Science Avenue, Kiev 03028, Ukraine*

Abstract

For the contact of two finite portions of interacting rigid crystalline surfaces, we compute the the pinning energy barrier dependency on the misfit angle and contact area. This simple model allows us to investigate a broad contact-size and angular range, thus obtaining the statistical properties of the energy barriers opposing sliding for a single asperity. These data are used to generate the distribution of static frictional thresholds for the contact of polycrystals, as in dry or even lubricated friction. This distribution is used as the input of a master equation to predict the sliding properties of macroscopic contacts.

Keywords: tribology, mechanical contacts, atomic scale friction, boundary lubrication, relative crystalline orientation, size scaling

1. Introduction

In a regime of dry friction or boundary lubrication of a single contact, such as studied by atomic force microscope (AFM) techniques, the friction force depends substantially and nontrivially on the relative crystalline orientation of the facing surfaces, as was demonstrated experimentally by Dienwiebel *et al.* [1]. Special angles lead to superlubric sliding, but tend to be energetically unfavorable [2]. Depending on the contact mechanical details and the sliding speed, such superlubric orientations could have long enough time to reconstruct, approaching a state with a lower free energy but characterized by a higher barrier (aging), or be retained for long enough for them to provide a substantial superlubric contribution to the overall sliding dynamics. The connection between the nanoscale, where friction occurs through the breaking and formation of local contacts, and the meso- or macroscale, where many breaking junctions interact elastically, is commonly described by earthquake-type models [3, 4, 5, 6, 7, 8], or by a master equation approach [4, 9, 10, 11, 12], or by models inspired to the Greenwood-Williamson one [13, 14] such as the sub-boundary lubrication

*Phone: +39 02 50317355; Fax: +39 02 50317482; email: nicola.manini@mi.infm.it

**email: obraun.gm@gmail.com

model [15, 16, 17]. Except the case of ideally flat surfaces such as mica in surface-force apparatus (SFA) experiments, contact is always realized at microscopic asperities, whose size ranges typically in the nanometer to micrometer range. Even when a lubricant is present at the contacting asperities, in a boundary or sub-boundary lubrication context, the residual lubricant is often frozen by pressure and confinement, and hydrodynamic viscous sliding is replaced by a static (stick-slip) contact-breaking regime, which we focus on in the present work. In the multiasperity contact, where relative orientation of individual asperities is not really under control, the most important information to be extracted from a single-asperity model is the probability distribution $P_c(\varepsilon_a)$ of the slip activation barriers ε_a .

Molecular dynamics (MD) approaches to lubricated sliding friction [18, 19, 20, 21, 22, 23, 24, 25, 26, 27, 28] are usually forced to use some form of periodic boundary conditions (PBC) in order to prevent the escape of lubricant atoms (molecules) from the contacting region under high load, and to keep the simulation size under control. PBC mimic the infinite size limit, which might not be especially appropriate for sub-micrometer-size contacts between sliding surfaces. Moreover, a fully atomistic model would be computationally too demanding for a full statistical study of the size and angular dependency of the characteristics of contacts.

To study the contact, we introduce a simple rigid model for a finite-size breaking junction realized by the contact of a finite portion of two different crystalline surfaces. Such a rigid model could not possibly account for wear or for the dissipation occurring at contact breaking, as could MD simulations instead, but provides semi-quantitative estimates of the barriers opposing the onset of sliding, i.e., the static friction thresholds. The simple model allows us to evaluate the relevant statistical distribution of barrier energies. This distribution enters as a basic ingredient in the master-equation formulation, which, depending on the general shape of this distribution leads to different macroscopic sliding regimes, either stick-slip or smooth-sliding dynamics [9, 10].

The present paper reports progress beyond our MD study of Ref. [28]. For the MD simulations of that work, we used a fixed size of the contact area, and applied PBC to impose a given commensurability ratio with minimal boundary effects, and to obtain a fair comparison of different misfit angles ϕ . Of course, the friction force f , and in particular its dependency on the angle ϕ , does change with the system size. For a larger contact area, increasingly many incommensurate angles emerge, producing a more irregular dependency $f(\phi)$. In the limit of infinite size, $f(\phi)$ develops an infinite number of singularities [29], but this limit is not to be taken too seriously, since in practice a single contact of a given crystalline orientation never exceeds a fraction of μm^2 in practical experimental conditions.

A numerical determination of the size dependency of $f(\phi)$ would constitute a formidable task for MD simulations, since larger sizes are not only individually more expensive computationally, but would require a finer and finer sampling of angles ϕ and longer equilibration times. It is instead straightforward to obtain the size dependency of the rigid-island model. Thus, *the main goal of the present*

work is to find, at least qualitatively, the shape of the distribution of static thresholds $P_c(\varepsilon_a)$, which is the main input of the master-equation approach to friction on meso/macro-scale, for a contact of polycrystalline surfaces.

In Sec. 2 we spell out the details of this rigid-contact model for the analysis of the static friction barrier realized by the contact of a crystalline surface with the boundary lubricant layer, which we assume in a close-packed ordered configuration. Sections 3 and 4 discuss the angle and size dependency of the friction of a nanocontact, and we compare our results with those of the MD lubricated model [28]. The basic implications for macroscopic sliding are discussed in Sec. 5 within a master-equation approach. Section 6 summarizes and discusses our results.

2. The rigid-island model

We represent the sliding contact, or the solidified boundary lubricant at the contact, with a finite rigid crystalline layer of lattice constant a , consisting of N point-like atoms. We put it in interaction with a substrate potential which is also rigid and periodic, e.g., a sinusoid of a generally different period a_s and amplitude V_0 . In the case of a one-dimensional system, one can easily find an explicit expression for the activation energy barrier for the onset of motion along the chain:

$$\varepsilon_a = V_0 \left| \frac{\sin(2\pi Na/a_s)}{\sin(2\pi a/a_s)} \right|. \quad (1)$$

Accordingly, for suitable values of the lattice constant, namely for $a = n a_s / (2N)$ with integer n (but not a multiple of N), this activation barrier vanishes and the chain moves freely. For a nonrigid layer, the activation energy remains nonzero for all values of a , but still reaches the first minimum at $a/a_s \propto 1/N$: the motion in such a case is of a “caterpillar” type (for details see Refs. [30, 31]).

A two-dimensional “lubricant” island advancing over the 2D periodic substrate should exhibit a similar behavior: in particular, a minimum for the activation energy is expected at $a/a_s \propto 1/\sqrt{N}$. The 2D system, however, has one extra degree of freedom, the rotation. We expect that the activation energy would achieve minima for specific misfit angles.

To investigate this pattern of minima, we consider a rigid island of size N with a triangular lattice interacting with the simplest 2D substrate periodic potential

$$V(x, y) = V_0 (\sin x + \sin y) \quad (2)$$

of square symmetry and lattice spacing $a_s = 2\pi$. The atomic coordinates of the approximately square-shaped island are $\tilde{x}_{i,j} = X + (i + j/2)a$ and $\tilde{y}_{i,j} = Y + jh$, where $h = a\sqrt{3}/2$, and the indexes $i = -j/2, \dots, -j/2 + n_i - 1$, $j = 0, \dots, n_j - 1$. The number of atoms in the rigid flake is $N = n_i n_j$, with $n_i a \approx n_j h$. X and Y are the degrees of freedom for the translation of the rigid island. If we rotate the island by an angle ϕ , then the atomic coordinates change to

$x_{i,j} = \tilde{x}_{i,j} \cos \phi - \tilde{y}_{i,j} \sin \phi$ and $y_{i,j} = \tilde{x}_{i,j} \sin \phi + \tilde{y}_{i,j} \cos \phi$. For a fixed misfit angle ϕ , the total potential energy of the island in contact with the substrate is

$$U(X, Y) = \sum_{j=0}^{n_j-1} \sum_{i=-j/2}^{n_i-1-j/2} V(x_{i,j}, y_{i,j}). \quad (3)$$

The set of stationary points of $U(X, Y)$, defined by

$$\partial U / \partial X = 0 \quad \text{and} \quad \partial U / \partial Y = 0, \quad (4)$$

consist of four elements: one minimum U_m , two saddle points U_{s1} and U_{s2} , and one maximum. The nature of the stationary points can be verified by computing the Hessian of $U(X, Y)$ at each stationary point, but it is in fact simply provided by the values of the function at the points. The activation energy for sliding is

$$\varepsilon_a = U_s - U_m, \quad (5)$$

where the lower saddle energy $U_s = \min(U_{s1}, U_{s2})$ is considered. The calculation of the energy barrier ε_a is extremely fast and efficient, since it only requires the search of the stationary points in a 2D space, by solving a simple numerical equation (4). Given the simplicity of this model, it allows us to compute ε_a for a very fine sampling of angles and contact sizes, as would be practically impossible if a fully atomistic simulation is used. Note that the computed barrier height is relevant irrespective of the direction in which the rigid island is pushed forward.

Although not completely equivalent, the activation energy barrier is indeed related to the threshold force f_s necessary to initiate sliding. To compare the results of the present rigid-island approach with the fully atomistic simulations of Ref. [28], we take $a/a_s = 4.14/3$, and assume that $f_s = \kappa \varepsilon_a / a_s$, where κ is a factor of order unity. This comparison is shown in Fig. 1 for an intermediate island size. We see that, at least qualitatively, MD and the present simple rigid model agree on predicting static-friction minima near a set of ‘‘special’’ angles. The singularities at the optimal angles are exact zeroes for the rigid model: here the two lowest stationary points of $U(X, Y)$ mutate into a degenerate trough. Unfortunately, within the PBC setup of MD it is impossible to cover such a fine sampling of misfit angles as allowed by the rigid model one: it is thus impossible to verify to what extent the two models agree or disagree on the specific superlubric angular orientations. The purpose of this comparison is purely to highlight a general qualitative similarity of the outcomes of two models, which are distinct and address significantly different physics. The main difference between the rigid model and the deformable lubricant film is that the deformable model has a finite barrier against sliding for all angles, even at optimal ones.

3. Barrier versus misfit angle

Figure 2 shows the angular dependency of the barrier against sliding $\varepsilon_a(\phi)$, for different sizes of the sliding island. The barrier reaches its first minimum at

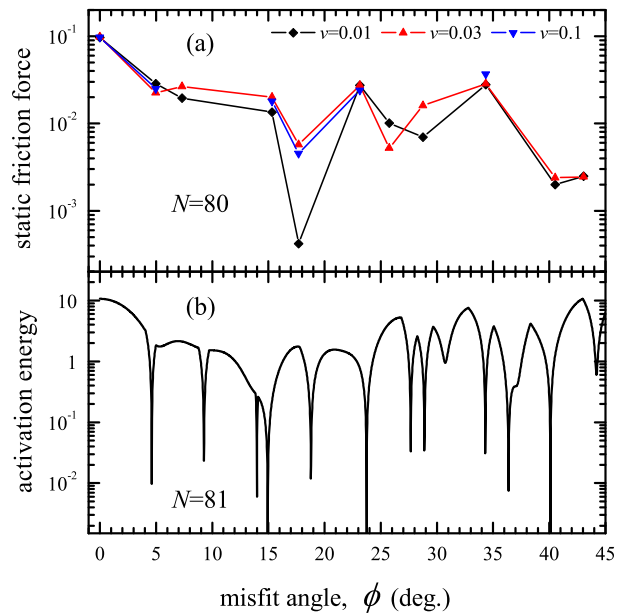


Figure 1: (Color online) (a) The static friction force (immediately before slip) as a function of the misfit angle ϕ for a one-layer lubricant film at zero temperature for different driving speeds, computed with MD simulations with in-plane PBC [28]. The friction force and driving speed are given in natural model units, of the order 1 nN and $\simeq 1$ m/s respectively. For full details on these simulations, see Ref. [28]. (b) The activation energy ε_a (units of V_0) for the sliding of a rigid island composed of $N = 81 = 9 \times 9$ lubricant atoms over the rigid square substrate as a function of ϕ .

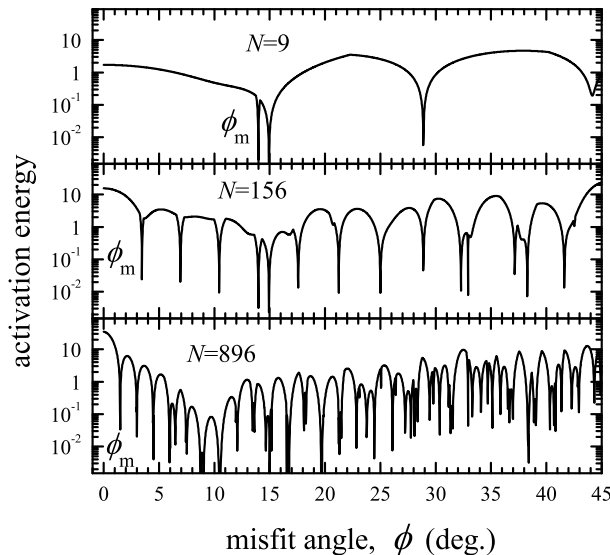


Figure 2: The activation energy ε_a (units of V_0) as a function of the misfit angle ϕ for three rigid lubricant islands composed by $N = 9$, 156 and 896 atoms.

a misfit angle $\phi_m \approx \pi/(4\sqrt{N})$, which moves to smaller and smaller angle as the size N of the island grows.

Figure 3 shows that high barrier energies ε_a correlate well with rather stable configurations characterized by a low minimum energy U_m , while low-barrier superlubric angles are usually characterized by unstable (high U_m) configurations. A higher stability of a given angular configuration could make that configuration more likely, if the asperity is free to rotate. We take this correlation into account when we evaluate the distribution of depinning thresholds in the rigid model, based on the evaluation of ε_a over a fine grid of angles, as illustrated by Fig. 4. For a given contact size N , the distribution of activation barriers exhibits weak divergences produced by the round maxima of $\varepsilon_a(\phi)$, plus jump discontinuities produced by the “kinky” maxima associated to a crossing of the saddle points, as illustrated for two sizes by the comparison of Figs. 3 and 4.

If the individual contacts are allowed the freedom and a sufficiently long time to rotate, thermal fluctuations will lead to geometric relaxation, eventually leading to an appropriate angular distribution $P_\phi(\phi)$; if one can neglect the interaction of the contacting grain with the rest of the slider, this distribution should match a Boltzmann distribution $P_\phi(\phi) \propto \exp[-U_m(\phi)/k_B T]$ of the fully relaxed energy U_m of the grain-substrate interaction. If, on the contrary, misfit angles are frozen by the microcrystalline nature of the surfaces in contact for much longer than the time of the experiment, all angles are equally likely and $P_\phi(\phi)$ is a constant (equivalent to the limiting Boltzmann distribution for $T \rightarrow \infty$). Averaging with these two different weight patterns leads to related but significantly different distributions, as illustrated by the comparison of dashed

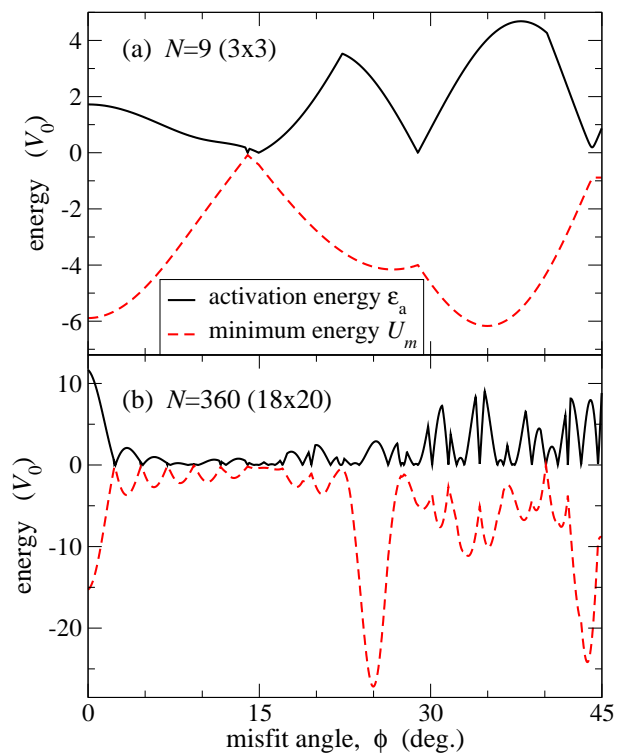


Figure 3: (Color online) A direct comparison of the energy U_m of the minimum (dashed) with the activation barrier ϵ_a (solid), as functions of the misfit angle ϕ for two sizes of the rigid island. Energies are in units of the substrate potential corrugation V_0 .

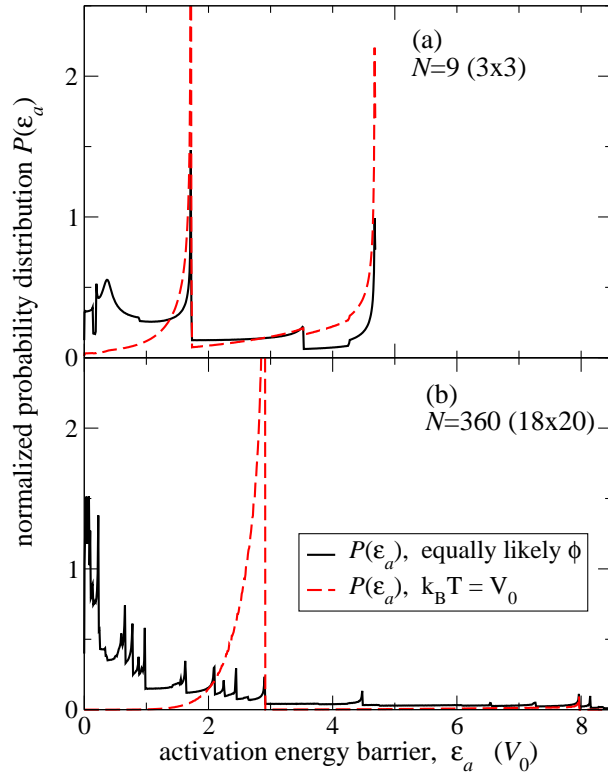


Figure 4: (Color online) The distribution of activation barriers ϵ_a for two island sizes reported in the corresponding panels of Fig. 3. The solid line is computed assuming all misfit angles ϕ are equally likely, the dashed line weights different angles according to a Boltzmann distribution of the corresponding minimum energy U_m , for a temperature $k_B T = V_0$ matching the typical potential barrier of a single lubricant particle.

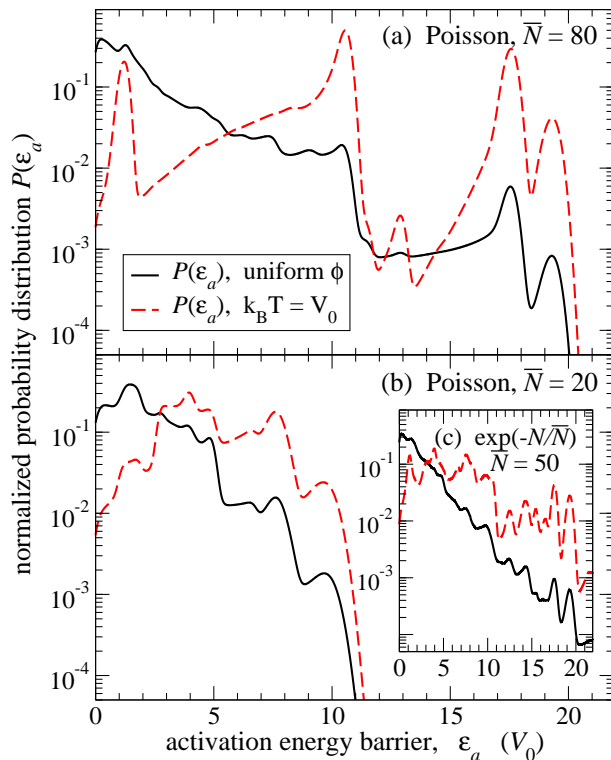


Figure 5: (Color online) The probability distribution of static thresholds for the rigid domains averaged over the domain size N with the Poissonian distribution of average domain size (a) $\bar{N} = 80$ and (b) $\bar{N} = 20$. Inset (c): the probability distribution computed by averaging over an exponential size distribution $\exp(-N/\bar{N})$ with $\bar{N} = 50$. Averaging over the misfit angle ϕ is carried out for solid (all angles are presented equally likely) and dashed (different angles are weighted according to the Boltzmann distribution) lines as in Fig. 4.

and solid lines in Fig. 4. Observe in particular that the effect of the Boltzmann weights is to suppress the probability of small activation barriers ε_a : this is a consequence of the stable angles (minima of U_m) being typically associated to high barriers ε_a , as remarked above (see Fig. 3). If the atomic layer represents a frozen lubricant, then one should beware of other ϕ -dependent energy contributions to be added to U_m due to the interaction with the crystalline anisotropy of the asperity region of the upper slider. These extra terms would of course influence the Boltzmann weights in the fast-rotating condition, in a way which could only be predicted in a condition where the details of this interaction and relative crystalline alignment were given.

4. The distribution of static thresholds

To describe friction in a meso- or macroscopic multi-contact regime it makes sense to assume a distribution of contact sizes N , and obtain the statistical

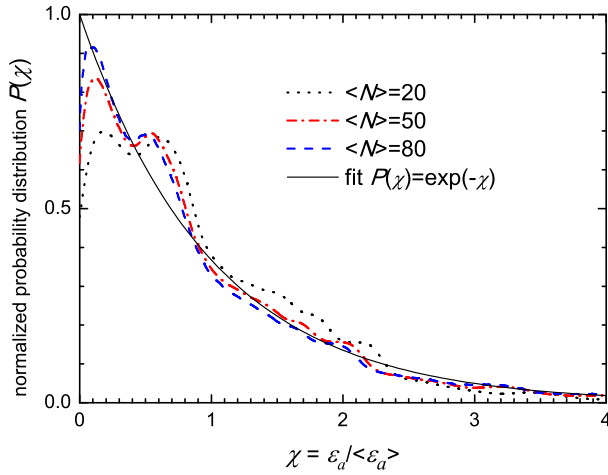


Figure 6: (Color online) The probability distribution of static thresholds $P_c(\chi)$ as a function of renormalized barrier heights $\chi = \varepsilon_a / \langle \varepsilon_a \rangle$ for the rigid domains averaged over the domain size N with an exponential size distribution $\exp(-N/\bar{N})$ with $\bar{N} = 20$ (dotted/black), 50 (dot-dashed/red) and 80 (dashed/blue).

contact properties by averaging over N . For the size distribution one may take a Poisson distribution $P(N) = (\bar{N}^N / N!) \exp(-\bar{N})$ with an average domain size \bar{N} . We include clusters of nearly squared shape only.

By combining this size distribution with the distributions of unpinning barriers for individual sizes N , calculated in the previous Section, we obtain a global distribution of barrier heights. The resulting distribution is displayed in Fig. 5, where we have smoothed the singularities of the distribution for each individual size N by means of the convolution with a Gaussian of full width at half maximum matching the average inter-peak spacing (varying from $0.1 V_0$ to $2.5 V_0$). We see that this distribution decays roughly exponentially by approximately two decades, and then drops rapidly due to the fast large-size decay of the Poisson function combined with the decreasing probability of barriers of increasing height, as illustrated in Fig. 4b. The choice of a Poisson distribution is not especially critical: a similar distribution of static thresholds is obtained if we assume an exponential size distribution $P(N) = \bar{N}^{-1} \exp(-N/\bar{N})$, see Fig. 5c.

The comparison of panels (a) and (b) of Fig. 5 shows that the average contact size \bar{N} affects the quantitative detail of the distribution, but not its qualitative shape. Moreover, if we plot the individual distributions as functions of the dimensionless rescaled activation energy barrier

$$\chi = \varepsilon_a / \langle \varepsilon_a \rangle, \quad (6)$$

all distributions may be roughly approximated by the exponential function $P_c(\chi) = \exp(-\chi)$ as demonstrated in Fig. 6. Remarkably, the general shape of the distribution of barriers of the rigid-island model resembles the distribu-

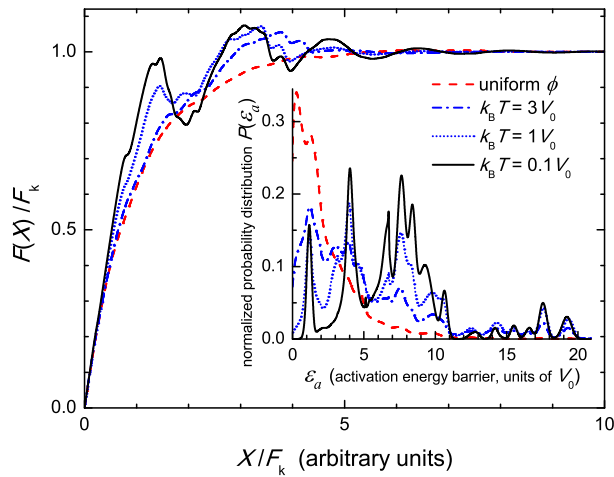


Figure 7: (Color online) The friction force $F(X)$ (normalized on the $X \rightarrow \infty$ limiting value F_k , corresponding to the kinetic friction force in the smooth-sliding regime) as a function of the displacement X of the rigid slider for different distributions of static thresholds shown in inset. Inset: the probability distribution of static thresholds for the rigid domains averaged over the domain size N with an exponential size distribution $\exp(-N/N)$ with $\bar{N} = 50$, when averaging over the misfit angle ϕ is weighted according to a Boltzmann distribution of the domain energy, for different temperatures.

tion, shown in Fig. 9 of Ref. [28], of static thresholds in the lubricated model based on PBC and a single size $N = 80$. The main visible difference is that, for the deformable domains of Ref. [28], the probability of small barriers is significantly lower than for the rigid slider at hand.

Small barriers ε_a become also suppressed when the islands can rotate so that angles are distributed thermally. As temperature decreases, the distribution of static thresholds exhibits more and more pronounced local maxima at values corresponding to minima of the domain's potential energy (see inset of Fig. 7).

5. Consequence for macroscopic sliding

Once the distribution of static thresholds is known, we can predict the dynamics of the tribological system with the help of the master-equation approach based on an earthquake-like model [9, 10, 11]. Consider the contact of two rough unlubricated substrates (top and bottom) on a meso- or macroscale. If the position of the bottom substrate is kept fixed and the top substrate is displaced by a distance X , the interface force (shear stress) begins to grow, $F \propto X$. Then, the domains where the stress exceeds a corresponding threshold value, start to slide, thus relaxing the local stress, and the increase of the total force F will degrade. The overall average dependence $F(X)$ follows from a solution of this master equation, where the distribution of static thresholds is the input parameter, as discussed in detail in Refs. [9, 10, 11].

For the threshold distributions calculated above, typical dependences $F(X)$ are shown in Fig. 7. When the misfit angles are distributed equally likely so that the distribution of static thresholds is nonzero down to zero threshold and $P_c(\varepsilon_a)$ has no sharp maxima, the force F increases monotonically with X , approaching the kinetic-friction force F_k characteristic of smooth sliding for $X \rightarrow \infty$. Thus, in such kind of macroscopic slider, static and kinetic friction forces coincide, and the motion always corresponds to smooth sliding. In contrast, when the threshold distribution exhibits well pronounced sharp maxima, like for thermalized domains or for an ordered homogeneous thin lubricant film, the function $F(X)$ reaches a maximum (which represents the macroscopic static friction force F_s) greater than F_k , and then decreases as the asperities give way collectively. For a soft enough slider, the inequality $dF(X)/dX < 0$ for some X leads to the appearance of the elastic instability in the system dynamics [9, 10]. Under such conditions, the macroscopic slider may exhibit stick-slip motion, provided the slider is soft and the delay in contact reformation is taken into account [11].

6. Discussion and Conclusion

The calculations within the simple model at hand provide, first of all, relevant insight for a single-asperity microscopic system, e.g. for a flake sliding over an atomically flat surface, where the slider may rotate and search for a local minimum of the potential energy. As a consequence, even if sliding starts off in a low-friction state (e.g., in the superlubric state associated to a highly incommensurate ϕ [1]), the flake will eventually rotate and spend most of its time near a local minimum (Fig. 3 indicates that for the triangle-on-square geometry of the present model such minimum need not be $\phi = 0$). Accordingly, after a relaxation time typical of the flake rotation, friction should increase (as predicted by the low- ε_a side drop of the distribution of Fig. 5). Such a behavior was observed experimentally and in MD simulation [2]. Observe also that an increased rate of thermally activated jumps across the pinning barriers would additionally lead to a thermolubric regime [32, 33].

More than single-asperity experiments, the focus of the present work concerns meso- and macroscopic sliding friction. At the nanoscopic level, the friction force produced by a sliding contact depends substantially and nontrivially on the relative crystalline orientation of the facing surfaces. In the present work we provide a basic tool to connect between the nanoscale, where friction occurs through the breaking and formation of local contacts, and the meso/macro-scale, where many breaking junctions interact elastically, as commonly described by an earthquake-type model or by a master-equation approach. The quantity that summarizes the information obtained by averaging over all possible contact sizes and angles is a probability distribution $P_c(\varepsilon_a)$ of the slip activation barriers ε_a . Our simple model permits us to evaluate such a distribution of barrier energies, reaching beyond the small sizes and few rotation angles allowed by detailed microscopical MD simulations. This distribution is a basic ingredient for the master-equation formulation, which, depending on the actual shape of this distribution can lead to different general macroscopic sliding regimes. The

analysis of the shape of this distribution allows one to understand the physics of the meso-macroscopic sliding in terms of the underlying microscopic junction-breaking statistical properties.

Two basic regimes of macroscopic sliding emerge from this model: (i) When superlubric alignments are suppressed by aging to thermodynamically more favorable alignments, a nonmonotonic peaked distribution $P_c(\varepsilon_a)$ of barrier heights is obtained, which tends to induce a macroscopic stick-slip regime. (ii) In contrast, when the probability of weak activation barriers is sufficiently large to produce a monotonically decaying distribution $P_c(\varepsilon_a)$, then macroscopic smooth sliding is possible, even in the presence of microscopic breaking-junction dynamics.

The present simple and very idealized model is not meant to address any specific properties of a well-defined contacting system, but it focuses on the possibility to extract macroscopic statistical information out of the mechanical properties of contacts. Many details of real contacts are left out, including surface curvature, wear, local thermal expansion. For this reason, it would be interesting (although extremely expensive numerically) to attempt a similar statistical method using the MD simulations of a specific contact described in terms of realistic force fields and curved surfaces. While the quantitative detail of $P_c(\varepsilon_a)$ is likely to depend on the specific contacting materials, its general properties should mostly follow those determined by means of the present simple model.

Acknowledgments

We wish to express our gratitude to B.N.J. Persson for helpful discussions. This research was supported in part by a grant from the Cariplo Foundation managed by the Landau Network – Centro Volta, and by the Italian National Research Council (CNR, contract ESF/EUROCORES/FANAS/AFRI), whose contributions are gratefully acknowledged.

References

- [1] M. Dienwiebel, G.S. Verhoeven, N. Pradeep, J.W.M. Frenken, J.A. Heimberg, and H.W. Zandbergen, *Phys. Rev. Lett.* **92**, 126101 (2004).
- [2] A.E. Filippov, M. Dienwiebel, J.W.M. Frenken, J. Klafter, and M. Urbakh, *Phys. Rev. Lett.* **100**, 046102 (2008).
- [3] Z. Olami, H.J.S. Feder, and K. Christensen, *Phys. Rev. Lett.* **68**, 1244 (1992).
- [4] B.N.J. Persson, *Phys. Rev. B* **51**, 13568 (1995).
- [5] O.M. Braun and J. Röder, *Phys. Rev. Lett.* **88**, 096102 (2002).
- [6] A.E. Filippov, J. Klafter, and M. Urbakh, *Phys. Rev. Lett.* **92**, 135503 (2004).

- [7] O.M. Braun, I. Barel, and M. Urbakh, Phys. Rev. Lett. **103**, 194301 (2009).
- [8] I. Barel, M. Urbakh, L. Jansen, and A. Schirmeisen, Phys. Rev. Lett. **104**, 066104 (2010).
- [9] O.M. Braun and M. Peyrard, Phys. Rev. Lett. **100**, 125501 (2008).
- [10] O.M. Braun and M. Peyrard, Phys. Rev. E **82**, 036117 (2010).
- [11] O.M. Braun and E. Tosatti, Europhys. Lett. **88**, 48003 (2009).
- [12] M. Srinivasan and S. Walcott, Phys. Rev. E **80**, 046124 (2009).
- [13] J.A. Greenwood, J.B.P. Williamson, Proc. R. Soc. Lond. A **295**, 300 (1966).
- [14] J.A. Greenwood, C. Putignano, and M. Ciavarella, Wear **270**, 332 (2011).
- [15] A. A. Polycarpou and Izhak Etsion, J. Tribol. **120**, 296 (1998).
- [16] A. A. Polycarpou and I. Etsion, Tribol. Trans. **41**, 217 (1998).
- [17] N. Yu, S. R. Pergande, and A. A. Polycarpou, J. Tribol. **126**, 626 (2004).
- [18] M. R. Sørensen, K. W. Jacobsen, and P. Stoltze, Phys. Rev. B **53**, 2101 (1996).
- [19] B.N.J. Persson, *“Sliding Friction: Physical Principles and Applications”* (Springer-Verlag, Berlin, 1998).
- [20] O.M. Braun and A.G. Naumovets, Surf. Sci. Reports **60**, 79 (2006).
- [21] M.H. Müser and M.O. Robbins, Phys. Rev. B **61**, 2335 (2000).
- [22] G. He and M.O. Robbins, Phys. Rev. B **64**, 035413 (2001).
- [23] G. He and M.O. Robbins, Tribology Lett. **10**, 7 (2001).
- [24] I. E. Castelli, N. Manini, R. Capozza, A. Vanossi, G. E. Santoro, and E. Tosatti, J. Phys.: Condens. Matter **20**, 354005 (2008).
- [25] I. E. Castelli, R. Capozza, A. Vanossi, G.E. Santoro, N. Manini, and E. Tosatti, J. Chem. Phys. **131**, 174711 (2009).
- [26] F. Bonelli, N. Manini, E. Cadelano, and L. Colombo, Eur. Phys. J. B **70**, 449 (2009).
- [27] A.S. de Wijn, C. Fusco, and A. Fasolino, Phys. Rev. E **81**, 046105 (2010).
- [28] O.M. Braun and N. Manini, Phys. Rev. E **83**, 021601 (2011).
- [29] T. Gyalog and H. Thomas, Europhys. Lett. **37**, 195 (1997).
- [30] O.M. Braun, Surface Sci. **230**, 262 (1990).

- [31] O.M. Braun and Yu.S. Kivshar, “*The Frenkel-Kontorova Model: Concepts, Methods, and Applications*” (Springer-Verlag, Berlin, 2004).
- [32] K.B. Jinesh, S.Yu. Krylov, H. Valk, M. Dienwiebel, and J.W.M. Frenken, Phys. Rev. B **78**, 155440 (2008).
- [33] S. Yu. Krylov and J. W. M. Frenken, J. Phys.: Condens. Matter **20**, 354003 (2008).